Title

Magneto-Mechanical Optimization of Cross-Sections for $ \text{cos}(\theta)$Accelerator Magnets

Journal

IEEE Transactions on Applied Superconductivity, 32(6)

ISSN

1051-8223

Authors

Vallone, G

Auchmann, B

Maciejewski, M

et al.

Publication Date

2022

DOI

10.1109/tasc.2022.3155528

Magneto-Mechanical Optimization of Cross-Sections for cos(θ) Accelerator Magnets

G. Vallone, B. Auchmann, M. Maciejewski, J. Smajic

***Abstract*—The cross-section design of cos(θ) superconducting magnets is historically developed in a two-step process: initially, the coil geometry is defined on the basis of magnetic optimizations; then, the structure is designed around the coil. The first step searches for the best coil cross-section maximizing the magnetic field, margin, field quality and conductor efficiency. The latter step aims at limiting the coil stresses and deformations. However, the coil design, defined with the initial magnetic optimization, can influence the mechanical behaviour of the magnet, altering, for example, the peak stress during operation. As the critical current is a function of the applied strain, the mechanical implications of the coil cross-section design can limit the achievable performance. In this paper we propose an integrated optimization process that targets the peak stress on the conductor in addition to the magnetic objectives. The results are presented for a sample high-field Nb_3Sn dipole: a 4-layer design aiming at ultimate conductor performance.**

***Index Terms*—Superconducting magnets, Cross-Section optimization, Mechanical aspects**

I. Introduction

The development of superconducting magnets for particle accelerators has always dealt with stringent requirements on magnetic field strength and quality. This led to the development of ad-hoc codes that would maximize the central field and field quality, while minimizing the amount of conductor necessary. One example, widely used in the accelerator magnet community, is Roxie [1].

This design strategy was well suited for conductors that were not strongly sensitive to stress within their range of application, as for example NbTi. However, it might be less suited for fragile conductors like Nb_3Sn . For these conductors, the mechanical limits are also very stringent, as are the magnetic ones. When the field quality is not as important (e.g. test facility magnets), the mechanical limits of the conductor were considered in an iterative design process for the coil cross-section [2], [3]. In this process, the coil shape was optimized in an attempt to minimize the total stress on the conductor at all stages. This manual iterative approach, is feasible mostly when the optimization objectives are few (e.g. load line margin at a target field, peak stress on the conductor). This is not the case for accelerator magnets where the optimization attempts to minimize also several multi-poles. It is further complicated in cos(θ) designs, where the amount of degrees freedom is much larger with respect to the block design. Probably because of these challenges, in most cases, the coil cross-section was designed only after a magnetic optimization, and then the mechanical structure was designed around trying to limit the peak conductor stresses.

In this paper, we try to show that this standard approach of designing magnets might not find the optimal solution, as it might be possible to obtain similar magnetic performances with different peak stresses in the coil cross-section. The scope of this paper is not to propose the optimal cross-section for any particular cos(θ) magnet, but to show that, given a particular set of parameters, the solution obtained from the magneto-mechanical optimization can be superior to the one obtained from the traditional sequential process. In fact, the design space can be widely different for different use cases, as well as the relative weight of, for example, conductor cost and margin.

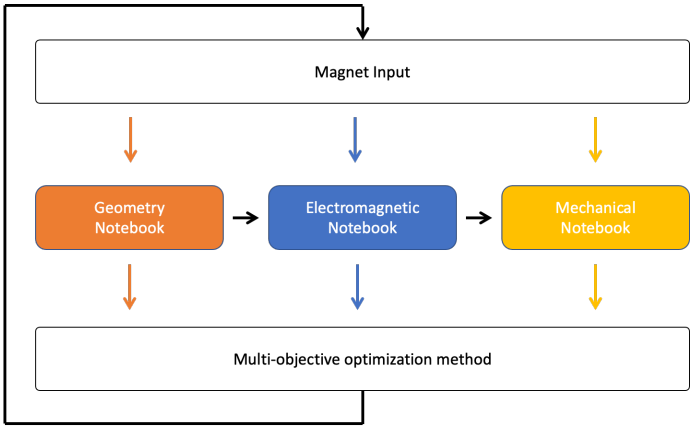

Fig. 1. Magneto-mechanical optimization flowchart.

II. Optimization process

The optimization process was implemented in the MagNum software package [4], following the flowchart shown in Fig. 1. For a selected space of magnet parameters, the software generates a cross-section geometry as a function of the cable geometry and layer parameters. The cross-section is checked against physical constraints on the design space (e.g. the turns do not overlap, are all on the first quadrant etc.). If all the checks are passed, the magnet information is then translated as input for the electromagnetic and mechanical models. The

Automatically generated dates of receipt and acceptance will be placed here
This work was supported by the US Department of Energy, Office of Nuclear Science

G. Vallone is with Lawrence Berkeley National Laboratory, Berkeley, CA 94720 USA (e-mail: gvallone@lbl.gov).

B. Auchmann is with Paul Scherrer Institute, PSI CH, Forschungsstrasse 111, 5232 Villigen, Switzerland, and with CERN, Geneva, Switzerland.

M. Maciejewski and J. Smajic are with Institute of Electromagnetic Fields, ETH Zurich, Switzerland.

Colour versions of one or more of the figures in this paper are available online at http://ieeexplore.ieee.org.

Digital Object Identifier: xx

TABLE I
OPTIMIZATION OBJECTIVES

Parameter	Function
Load line margin	Quadratic
Peak equivalent stress	Quadratic
b_3	Quadratic
b_5	Quadratic
Conductor area	Linear
Cable radiality	Linear

electromagnetic simulation, implemented in ROXIE, is run first, and used to generate the electromagnetic forces applied to the mechanical model. More details on the mechanical model are provided in section II-B. Finally, the objective parameters are extracted from the models and used for the optimization process.

The optimization is defined as follows:

1) A superconducting cable is selected, defining geometry, strand and insulation parameters.
2) The work point of the magnet is defined, with a target field and load line margin.
3) The optimization function is defined (see next section).
4) The design space is defined setting the number of layers, and a range for the number of coil blocks, the number of conductors per layer, and the relative angles between the coil blocks.
5) A genetic optimization algorithm is used to investigate the design space trying to minimize the optimization function.

Clearly, step number 1 might be also added as part of the whole optimization process, but was not used for this work.

A. Optimization function

The selected optimization objectives are listed in Table I. As expected, among the selected objectives were the load line margin, field quality, and the maximum equivalent stress on the conductor. An additional parameter was used to track the the total conductor cross-sectional area. This allows to simply include a potential cost associated to the selected design. For 2 layer designs, this additional parameter might be removed, and the design is defined by targeting a particular load line margin. However, in designs that use 4 layers, this might favor solutions that favor a high number of cables on the outer layers. To prevent the selection of coil geometries that would not be easily windable in the end region, the deviations of the cables from the radial position are penalized.

The optimization function is simply defined as the sum of weighted functions f_i, defined for each optimization parameter p_i with either linear or quadratic functions. The optimization engine attempts to find the minimum of this function. The quadratic functions were corrected with piece-wise definition:

$$f_i = \alpha_i (p_i - t_i)^{\beta_i} \quad \text{if} \quad (p_i - t_i) > t_0 \tag{1}$$

$$f_i = \gamma_i p_i \quad \text{if} \quad (p_i - t_i) < t_0 \tag{2}$$

where t_i is the target for the parameter (e.g. required margin = 16%), α_i, β_i and γ_i are scaling weights. The value of these weights have to be carefully balanced in order to obtain a solution that is close enough to all the required targets. Splitting the function definition across the zero allows to avoid penalizing the solutions that are better than the target value. For values that can be negative, as for example the harmonics b_i, p_i is taken as their absolute value.

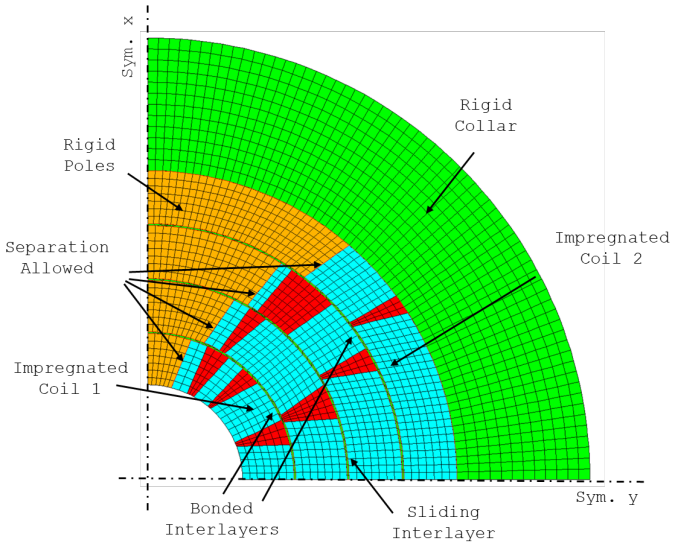

Fig. 2. Overview of the boundary conditions and contact conditions applied to the mechanical model.

TABLE II
MECHANICAL MODEL - MATERIAL PROPERTIES

Material	Ref.	Details	E, 4.5 K, GPa
Nb_3Sn Coil	[5]		25
Al. Bronze	[6]	C61400	112
Fiberglass	[7]	Parallel to the fibers	30
		Normal to the fibers	6

B. Mechanical model assumptions

The mechanical simulation was carried out with automatically generated ANSYS APDL scripts. The cross-section parameters are provided by a MagNum interface, that writes them on an human-readable file containing: number of layers, number of block per layer, corner positions of each blocks on an input file. Then, the code generates the superconducting coil, wedges, poles and interlayer rings. A rigid mechanical structure is added outside the last layer. Displacement boundary conditions were applied to prevent any motion of the structure and of the winding poles.. Contact elements are automatically generated to interface the coils and the structure. The wedges are considered bonded to the coils. The coil-pole interface is considered debonded from the start of the powering [8]. The interlayers can be bonded or sliding with respect to the coil depending on the assumptions. This allows, for example, to simulate bonded and non-bonded coils. A sliding with no friction condition is applied between the collar and the coil, to separate as much as possible the coil design from the one of the mechanical structure. Finally, symmetry boundary conditions are applied on the nodes laying on the horizontal and vertical

plane. A summary of the applied boundary conditions and contact conditions is provided in Fig. 2.

The material properties used are summarized in Table II. The wedges are made out of Aluminium Bronze, the interlayers and the filler of glass fiber reinforced plastic. The coil is assumed to be an uniform block with uniform isotropic properties. The coil modulus can play a key role in the stresses applied on the coil. In fact, the e.m. forces try to deform the coil in an ellipse as the thickness of the coil grows, the coil can start to bend and the peak stress can move from the outer radius of the coil to the inner layer. The amount of bending and relative stress at the inner radius of the innermost layer can grow when the modulus is reduced. Here we assume that the modulus is 25 GPa.

The solution is limited to a powering step where the e.m. forces, computed by Roxie, are applied to the nodes, using the roxie2ansys interface [9]. The stress generated by a potential cool-down and prestress are not represented in this model. Instead, a rigid structure is assumed to be around the coils. In theory, one could also pick a particular structure design and use it in the optimization process. But given the variety of these designs, this is not done here. Furthermore, the optimal support structure design might be a function of the particular cross section, and this would likely result in additional input parameters to be optimized. In general, a perfectly rigid structure will, in most cases, provide a solution that outperforms what is actually achievable in reality.

C. Speed considerations

For a 4 layer cos(θ) magnet design, a single genetic optimization run can consist of thousands of solutions. Furthermore, the optimization process can require subsequent runs, with human inputs, in order to refine the design space and guide the optimizer to the best solution. As a consequence, the solution speed is crucial to obtain an optimized solution in a reasonable time window. A typical electro-magnetic model can be solved, when neglecting the iron yoke, in less than a second on most commercial CPUs. A full solution would need to consider also the presence of the iron parts. This can significantly increase the solution time. Luckily, for most magnets, the contribution of the yoke to the magnetic field can be estimated (or computed) a priori and added as constant contribution to all designs. In the design process, the electromagnetic model was solved removing the iron contribution from the target field. The electromagnetic forces, needed for the mechanical model, were then linearly scaled from the computed value to a target field which considers also this constant iron contribution.

The mechanical model, on the other hand, requires a significantly larger time to solve, between 10 and 20 seconds on a single core of a modern CPU. Because of the relative small size of the model, adding parallel processing to the solution of a single model does not significantly reduce this solution time. To solve this, another strategy was developed, where multiple designs are solved in parallel. This allows to scale well the optimization process with the number of available processors.

TABLE III
STRAND AND CABLE PARAMETERS

	Layer 1, 2	Layer 3, 4
Strand Parameter	Value	
Wire Diameter [mm]	1.1	0.7
Cu to non-Cu ratio	1.17	2.2
J_c [A/mm^2]	887†	2359‡
Cable Parameter	Value	
Number of Strands	22	37
Width [mm]	13.2	13.65
Inner Thickness [mm]	1.892	1.204
Outer Thickness [mm]	2.0072	1.323
Insulation Thickness [mm]	0.15	0.15

† At 4.2 K, 18 T.
‡ At 4.2 K, 15 T.

TABLE IV
DESIGN SPACE (MIN, MAX)

	Layer 1	Layer 2	Layer 3	Layer 4
Number of conductors	(8, 14)	(12, 25)	(25, 35)	(25, 40)
Number of blocks	(2, 4)	(2, 3)	(2, 3)	(2, 3)
$\phi_{r_{12}}$	(1, 8)	(1, 8)	(1, 8)	(1, 8)
$\phi_{r_{23}}$	(1, 6)	(1, 5)	(1, 8)	(1, 8)
$\phi_{r_{24}}$	(1, 4)			
$\alpha_{r_{12}}$	(-6, 8)	(-5, 8)	(-6, 8)	(-6, 8)
$\alpha_{r_{23}}$	(-6, 6)	(-5, 8)	(-6, 8)	(-6, 8)
$\alpha_{r_{24}}$	(-6, 5)			

III. AN OPTIMIZATION EXAMPLE: A 4 LAYER, 16 T COS(ϑ) DIPOLE

The design space for the 4 layer magnet optimization was defined using the assumptions used for the main bending dipole developed as part of the FCC design study [10]–[12]. The conductor specification were extracted from the FCC development wire [13], and are reported in Table III along with the cable parameters. Two different cables were assumed for the two inner layers (1, 2), and for the two outer layers (3, 4). The magnet targets a 16 T bore field. For the optimizer, a central field of 15 T was considered in the magnetic models, and, assuming that the iron will contribute to an additional 1 T, the e.m. forces were scaled to 16 T. The 4 layers were considered part of two separate coils: glued conditions were applied to the interlayers between layer 1 and 2, and layer 3 and 4; frictionless sliding conditions on the interlayer between layer 2 and 3. The actual contact condition at this interface depends on the coil construction process. Gluing the 4 layers together might increase the overall stiffness of the coil and further reduce the stresses on the conductor. The input parameters of the design space for the optimization are reported in Table IV. In the table, $\phi_{r_{ij}}$ is the relative angle between the blocks, and $\alpha_{r_{ij}}$ the angular deviation from

TABLE V
OPTIMIZATION RESULTS

	Margin† /	b_3 Units	b_5 Units	$\sigma_{equ_{max}}$ MPa
4 Layers Magnetic	15.6%	0.1	0.2	198
4 Layers Magneto-Mechanical	15.8%	0.3	0.2	158

† Load line margin.

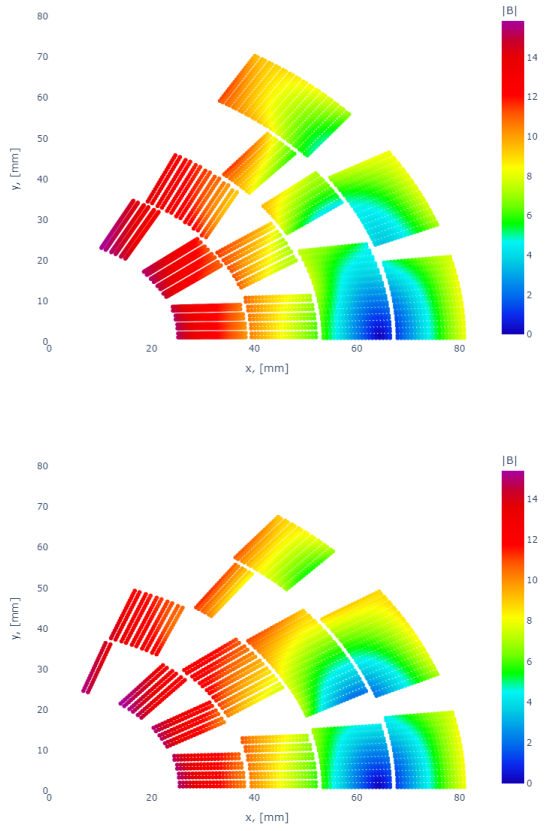

Fig. 3. 4 layer dipole: magnetic field on the strands after a pure magnetic optimization (top) and a joint magneto-mechanical optimization (bottom).

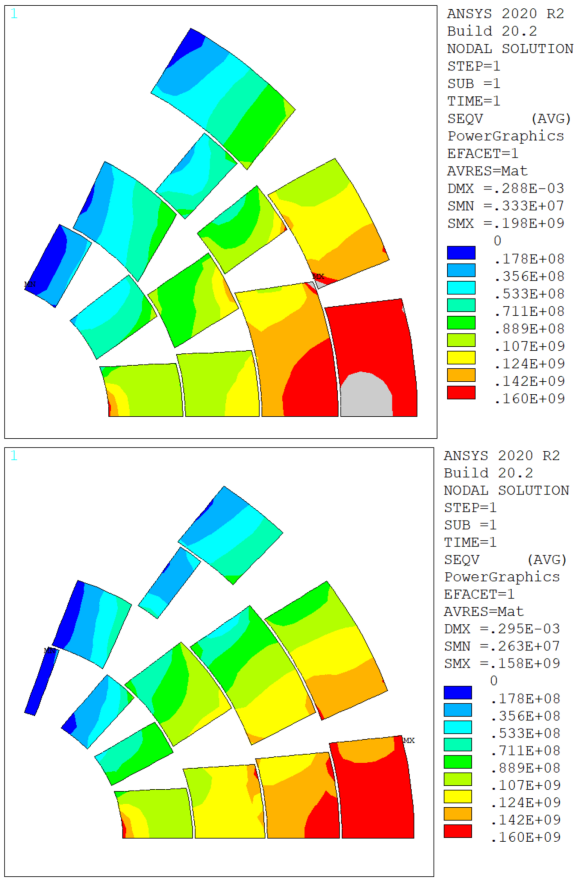

Fig. 4. 4 layer dipole: equivalent stress on the coils at 16 T, after a pure magnetic optimization (top) and a joint magneto-mechanical optimization (bottom).

a radial position of the first turn. The optimizer allows to keep the number of blocks as a parameter. The optimization objectives are reported in Table I.

The optimizer was run first neglecting the equivalent stress (magnetic optimization), and then considering it (magneto-mechanical optimization). The results of both optimization runs are reported in Table V. The field on the conductor is shown in Fig. 3 for both solutions. The field quality values are a bit high, but can be further improved with a fine optimization around the found solution. The margin is larger than the target of 15%. Equivalent stress contours for the two optimized cross-sections are shown in Fig. 4. At 16 T, the peak equivalent stress for this design is equal to 198 MPa for the magnetic optimization, and 158 MPa for the joint optimization. The peak stress of the magnetic optimization is located near a wedge tip, and due to local effects. This concentration might be limited to the cable insulation, not reaching the filaments, but could still result in damage at the interface between the wedge and the coils. On the midplane, the peak stress is equal to 170 MPa. This means that the joint optimization allows for a reduction of the peak stress of 20%, and about 10% if reduction when neglecting the stress concentration in the coil corners. The peak stress for the joint optimization is located on the outermost layer. However, the stress on the inner radius (high-field region) is also very close. It is likely that better designs could be obtained by considering separately the stress on the high field and the outer field region, and giving an higher weight to the former.

The optimization process reduces stress with two main strategies: aligning radially the wedges of different layers to allow for the e.m. load to be directly transferred to the outer structure; and placing a wedge in the middle of another layer to avoid stress concentrations and reduce the local overall bending. Further to this, the optimizer avoids solutions with stress spikes in the corners. These spikes might not be reaching the conductor in most cases, but can initiate crack propagation at the the wedges/cable interface. This can result, in turn, in a potentially dangerous deviation from the design condition.

IV. Conclusion

This paper proposed a new process to design cross-sections for accelerator magnets. The combined magneto-mechanical optimization allowed to reduce the peak stresses on the conductor during powering of about 10%.

The optimization process allowed to highlight interesting features of designs that provide lower stresses to the conductor. Results suggest that the wedges should be placed either in the middle of conductor blocks of adjacent layers, to increase the overall coil stiffness, or aligned radially, so that the e.m. forces can ‘flow’ towards the structure.

REFERENCES

[1] S. Russenschuck, "Roxie: A computer code for the integrated design of accelerator magnets," *accepted for presentation at COMPUMAG 2021, Cancun, Mexico*, 1999.

[2] G. Vallone *et al.*, "Magnetic and mechanical analysis of a large aperture 15 T cable test facility dipole magnet," *IEEE Transactions on Applied Superconductivity*, vol. 31, no. 5, pp. 1–6, 2021.

[3] M. Prioli *et al.*, "The CLIQ quench protection system applied to the 16 T FCC-hh dipole magnets," *IEEE Transactions on Applied Superconductivity*, vol. 29, no. 8, pp. 1–9, 2019.

[4] M. Maciejewski *et al.*, "Model-based workflows for multi-physics design optimization of superconducting accelerator magnets," *IEEE Transactions on Magnetics, Under Review*,

[5] C. Fichera *et al.*, "New methodology to derive the mechanical behavior of epoxy-impregnated Nb_3Sn cables," English, *IEEE Transactions on Applied Superconductivity*, vol. 29, no. 7, p. 8 401 912, 2019.

[6] H. J. Hucek, K. E. Wilkes, K. R. Hanby, and J. K. Thompson, "Handbook on materials for superconducting machinery, includes data sheets for first and second supplements, November 1975 and January 1977," Battelle Columbus Labs, Ohio Metals and Ceramics Information Center, Tech. Rep., 1977.

[7] C. L. Goodzeit, "Superconducting accelerator magnets - an introduction to mechanical design and construction methods," *USPAS*, 2001.

[8] G. Vallone and P. Ferracin, "Modeling coil-pole debonding in Nb_3Sn superconducting magnets for particle accelerators," *IEEE Transactions on Applied Superconductivity*, 2017.

[9] A Milanese, "A method to transfer distributed lorentz forces in 3D to a finite element mechanical model," *CERN-ATS-Note-2011-005*, 2011.

[10] A. Abada *et al.*, "Fcc physics opportunities: Future circular collider conceptual design report volume 1," English, *European Physical Journal C*, vol. 79, no. 6, p. 474, 2019.

[11] D. Tommasini *et al.*, "The 16 T dipole development program for FCC," *IEEE Transactions on Applied Superconductivity*, vol. 27, no. 4, pp. 1–5, 2017.

[12] M. Sorbi *et al.*, "The EuroCirCol 16 T cosine-theta dipole option for the FCC," *IEEE Transactions on Applied Superconductivity*, vol. 27, no. 4, pp. 1–5, 2017.

[13] S. Hopkins, "Status of conductor procurement," *FCC Magnets Collaboration Meetings - Kick-Off*, 2019.